Halo effects in the ^{11}Li$(p,t)^{9}$Li reaction

P. Descouvemont *

Physique Nucléaire Théorique et Physique Mathématique, Code Postal 229, Université Libre de Bruxelles (ULB), B 1050 Brussels, Belgium

(Received 5 May 2021; accepted 4 August 2021; published 16 August 2021)

I investigate the ^{11}Li$(p,t)^{9}$Li two-neutron transfer reaction at $E_{\rm lab} = 33$ MeV within the distorted wave Born approximation (DWBA). The ^{11}Li and ^{3}H nuclei are described in the hyperspherical formalism, as ^{9}Li $+n+n$ and $p+n+n$ configurations, respectively. The calculation of the cross section is shown to be much more complicated than in one-neutron transfer reactions, owing to the three-body structure of ^{11}Li. The ^{11}Li $+p$ and ^{9}Li $+t$ scattering wave functions are determined with the continuum discretized coupled channel (CDCC) method. Approximations derived from equivalent local potentials are used to compute the transfer cross section at the DWBA. The model reproduces experimental data reasonably well, considering that there is no adjustable parameter. I show that the cross section is fairly sensitive to the long-range part of the ^{11}Li wave function, and therefore to its halo structure.

DOI: 10.1103/PhysRevC.104.024613

I. INTRODUCTION

The study of halo nuclei is one of the main issues in modern nuclear physics [1]. In loosely bound nuclei, the neutron (or, in some cases, the proton) density extends far beyond the range encountered in tightly bound nuclei. This long-range density leads to specific properties of halo nuclei, such as an anomalously large radius [2]. A typical example is the ^{11}Li nucleus, which is considered as a ^{9}Li core surrounded by two neutrons with a separation energy of 0.378 MeV [3]. The ^{11}Li experimental radius is 3.16 ± 0.11 fm [4], which is much larger than the ^{9}Li radius (2.43 fm [5]).

The ^{11}Li nucleus has been studied in many experimental and theoretical works (see, for example, Ref. [6] and references therein). Owing to its short lifetime (8.6 ms), however, experimental data can be obtained through radioactive beams only. Consequently, the experimental information is generally deduced from reaction models. Typical examples are ^{11}Li elastic scattering on heavy targets [7] or on protons [8]. Breakup data are also widely used to assess ^{11}Li models [9].

The use of the ^{11}Li$(p,t)^{9}$Li two-neutron transfer reaction is more recent [10]. Two-neutron transfer cross sections were used in the past to investigate the structure of heavy nuclei (see, for example, Refs. [11–13]). Since the ^{11}Li nucleus is known to present a marked ^{9}Li $+n+n$ structure, this transfer reaction should be sensitive to the long-range part of the wave function. Reference [10] concludes that these data may give new insight on the halo structure of ^{11}Li, but that further studies are necessary.

The ^{11}Li $+p$ elastic scattering was recently studied [14] in the framework of the continuum discretized coupled channel (CDCC) method [15,16]. Elastic cross sections obtained at $E_{\rm lab} = 66$ MeV ($E_{\rm c.m.} = 5.5$ MeV) [8] were nicely reproduced by the CDCC approach, provided that ^{11}Li breakup effects are properly taken into account. The CDCC formalism was originally developed to describe $d+A$ reactions by including $p+n$ continuum states [15]. The continuum is simulated by positive-energy eigenvalues of the $p+n$ system, referred to as pseudostates. The application of the CDCC formalism to three-body projectiles is more recent [17,18]. It raises important numerical difficulties owing to the large number of pseudostates and to the long range of the coupling potentials. These issues can be solved nowadays with modern computer facilities and efficient numerical techniques.

The goal of the present work is to address the ^{11}Li$(p,t)^{9}$Li reaction with CDCC scattering wave functions. Of course, the transfer process is treated at the distorted wave Born approximation (DWBA; see Ref. [19]). The formalism is well known, even with CDCC wave functions [20], but the application to two-particle transfer is much more involved than to single-nucleon transfer reactions, such as (d,p) [21]. I describe ^{11}Li and ^{3}H in a three-body model (^{9}Li $+n+n$ and $p+n+n$, respectively), and these wave functions are used to compute the transfer cross section at the DWBA. It is then possible to investigate the role of the ^{11}Li wave function, and in particular of its long-range part, in the transfer process.

The paper is organized as follows. In Sec. II, I briefly present the three-body model used to describe ^{11}Li and t. I also give a short outline of the CDCC method. Section III is more specifically devoted to the calculation of the two-neutron transfer cross section at the DWBA. The application to ^{11}Li$(p,t)^{9}$Li is presented in Sec. IV, where I discuss halo effects in the transfer cross section. The conclusion and outlook are presented in Sec. V.

II. BOUND-STATE AND SCATTERING WAVE FUNCTIONS

A. Three-body model of ^{11}Li and ^{3}H

In the ^{11}Li$(p,t)^{9}$Li reaction, the ^{11}Li and ^{3}H nuclei are consistently described by a three-body model (^{9}Li $+n+n$

*pierre.descouvemont@ulb.be

and $p+n+n$, respectively). Their use in scattering calculations will be discussed in the next sections.

Let me consider the Hamiltonian of a three-body system

$$H_3 = \sum_{i=1}^{3} t_i + \sum_{i<j} v_{ij}(\boldsymbol{r}_i - \boldsymbol{r}_j), \tag{1}$$

where $\boldsymbol{r}_1, \boldsymbol{r}_2, \boldsymbol{r}_3$ are the coordinates of the particles (I take $\boldsymbol{r}_1$ as the core coordinate), and where v_{ij} are three interactions. An efficient technique to solve the Schrödinger equation associated with (1) is the hyperspherical formalism [22]. This method is well known in nuclear and in atomic physics, and I only outline the main principles. The reader is referred to Refs. [22–24] for more detail.

From the three coordinates $\boldsymbol{r}_i$, I define scaled Jacobi coordinates as

$$\boldsymbol{x} = \frac{1}{\sqrt{2}}\boldsymbol{r}_x, \quad \boldsymbol{y} = \sqrt{\frac{2A_1}{A_1+2}}\boldsymbol{r}_y, \tag{2}$$

with

$$\boldsymbol{r}_x = \boldsymbol{r}_3 - \boldsymbol{r}_2, \quad \boldsymbol{r}_y = \boldsymbol{r}_1 - \frac{\boldsymbol{r}_2+\boldsymbol{r}_3}{2}. \tag{3}$$

I assume a core nucleus with mass A_1, and two surrounding nucleons. The hyper-radius and hyperangle are defined as

$$\rho^2 = x^2 + y^2, \quad \alpha = \arctan\frac{y}{x}. \tag{4}$$

After removal of the center-of-mass coordinate, the three-body system is therefore described by five angles $\Omega_5 = (\Omega_x, \Omega_y, \alpha)$ and one hyper-radius ρ. Angular functions are defined, for a three-body system with total spin j, by

$$\mathcal{Y}^{jm}_{\gamma K}(\Omega_5) = \left[Y^L_{\ell_x\ell_y}(\Omega_x,\Omega_y) \otimes \chi^S_{S_{23}}\right]^{jm} \Phi_K^{\ell_x\ell_y}(\alpha), \tag{5}$$

where index γ stands for $\gamma = (\ell_x, \ell_y, L, S_{23}, S)$ and where K is the hypermoment (the parity is implied in j). In Eq. (5), I define

$$Y^{LM_L}_{\ell_x\ell_y}(\Omega_x,\Omega_y) = \left[Y_{\ell_x}(\Omega_x) \otimes Y_{\ell_y}(\Omega_y)\right]^{LM_L},$$
$$\chi^{SM_S}_{S_{23}} = \left[\chi_{S_1} \otimes \left[\chi_{S_2} \otimes \chi_{S_3}\right]^{S_{23}}\right]^{SM_S}, \tag{6}$$

where χ_{S_i} are spinors associated with the three particles. Functions $\Phi_K^{\ell_x\ell_y}(\alpha)$ are defined, for example, in Ref. [24].

The total wave function of the three-body system is expanded as

$$\Psi_3^{jm} = \rho^{-5/2} \sum_{\gamma K} \chi^j_{\gamma K}(\rho)\mathcal{Y}^{jm}_{\gamma K}(\Omega_5), \tag{7}$$

where the series over K is, in practice, truncated at some maximum value $K_{\max}$. Notice that the number of (γK) values increases rapidly with $K_{\max}$ and with j. The hyper-radial functions $\chi^j_{\gamma K}(\rho)$ are obtained from a coupled-channel system (see Ref. [24]), which is solved by expanding the hyper-radial functions over a set of N basis functions $u_i(\rho)$ as

$$\chi^j_{\gamma K}(\rho) = \sum_{i=1}^{N} c^j_{\gamma K i} u_i(\rho). \tag{8}$$

I choose $u_i(\rho)$ as Lagrange functions [24,25], which permit a simple and accurate calculation of the matrix elements. In practical applications, the number of γK values (or, in other words, of "channels") may reach 200–300 depending on j and on $K_{\max}$. The number of basis functions N is typically 30–40.

The potentials used to describe ^{11}Li are those adopted in Refs. [14,26]. The ^{9}Li $+n$ potential has a Woods-Saxon shape and contains a spin-orbit term [27] (the spin of the ^{9}Li core is neglected). The n-n interaction is taken as the central part of the Minnesota potential with the standard admixture parameter $u = 1$. The ^{9}Li $+n$ interaction is slightly renormalized (by a factor 1.0051) to reproduce the experimental [3] two-neutron binding energy $E_B = 0.378$ MeV. The rms radius of ^{11}Li is 3.12 fm, which agrees fairly well with experiment (3.16 ± 0.11 fm) [4]. The main components of the $j = 0^+$ wave function are obtained for $\ell_x = \ell_y = S = 0$ (61.4%) and for $\ell_x = \ell_y = S = 1$ (35.4%).

For ^{3}H, I use the n-n and p-n Minnesota potentials as in Ref. [28]. The binding energy is $E_B = 8.38$ MeV which is close to the experimental value 8.48 MeV. Since there is no tensor force, only $S = 1/2$ is present ($j = 1/2^+$). The dominant component is found for $\ell_x = \ell_y = 0$ (97.4%) with small components in $\ell_x = \ell_y = 2$ (1.2%) and in $\ell_x = \ell_y = 1$ (1.3%). The radius is 1.70 fm (neglecting the nucleon radius).

In Fig. 1, I present the ^{11}Li and ^{3}H wave functions in two ways. Figures 1(a) and 1(b) represent the dominant hyperspherical functions (7). As expected from the low binding energy, the ^{11}Li wave function slowly decreases at large ρ values. The main components are obtained for ($S = 0$, $K = 0, 2$) and for ($S = 1, K = 2$). The asymptotic behavior of the hyper-radial wave function is

$$\chi^j_{\gamma K}(\rho) \longrightarrow A^j_{\gamma K}(\kappa\rho)^{1/2} K_{K+2}(\kappa\rho), \tag{9}$$

where $\kappa = (2m_N E_B/\hbar^2)^{1/2}$, $K_n(x)$ is a modified Bessel function, and $A^j_{\gamma K}$ is an asymptotic normalization coefficient [29]. The asymptotic form (9) is reached beyond $\rho \approx 25$ fm.

The situation of ^{3}H is different since the binding energy is large and since the radial wave functions present a fast decrease. As the ^{11}Li$(p,t)^9$Li cross section involves some overlap between the ^{11}Li and ^{3}H wave functions, it is, however, important to pay attention to the long-distance behavior of ^{3}H.

Figures 1(c) and 1(d) provide a complementary view of the wave functions, with density probabilities defined by

$$P^j(r_x, r_y) = \int d\Omega_x d\Omega_y |\Psi^j(\boldsymbol{r}_x, \boldsymbol{r}_y)|^2. \tag{10}$$

Whereas ^{3}H presents a maximum at small $(\boldsymbol{r}_x, \boldsymbol{r}_y)$ values, the ^{11}Li wave function is maximum near $\boldsymbol{r}_x = 2.8$ fm and $\boldsymbol{r}_y = 3.1$ fm, and extends to large distances. These values are consistent with a large radius and with the well-established halo picture of ^{11}Li.

B. ^{11}Li + p elastic scattering

The ^{11}Li three-body wave functions are used in a CDCC calculation of ^{11}Li$(p,t)^9$Li scattering. The ^{11}Li$(p,t)^9$Li data of Ref. [10] are obtained at $E_{\rm lab} = 33$ MeV, which corresponds

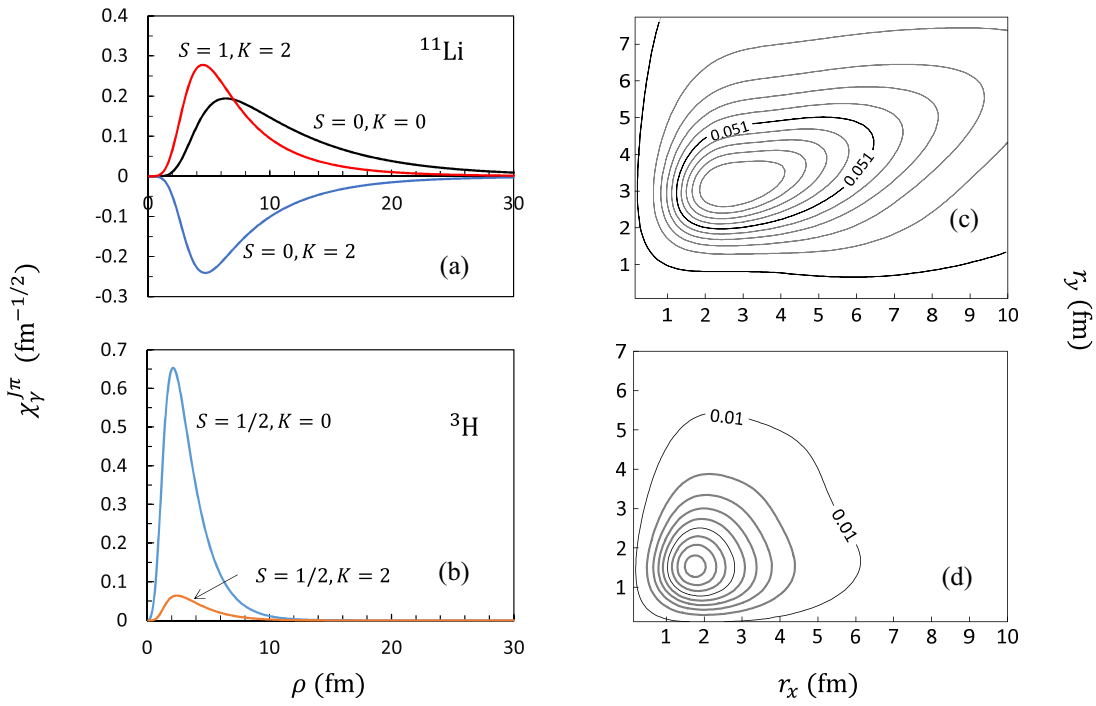

FIG. 1. ^{11}Li and ^{3}H three-body wave functions. Panels (a) and (b) display the hyperspherical functions defined in Eqs. (7) and (8), whereas panels (c) and (d) present the wave functions as contour plots [see Eq. (10)]. The steps between two contour lines in panels (c) and (d) are 0.01 and 0.05, respectively.

to a center-of-mass energy $E_{\text{c.m.}} = 2.75$ MeV. I follow the technique presented in Ref. [14].

The Hamiltonian of the $^{11}\text{Li} + p$ system reads

$$H = H_3 + T_{\boldsymbol{R}} + \sum_{i=1}^{3} v_{pi}(|\boldsymbol{R} - \boldsymbol{r}_i|), \tag{11}$$

where H_3 is the ^{11}Li Hamiltonian (1), $v_{pi}(S)$ are optical potentials between the proton and the constituents of ^{11}Li and where the relative kinetic energy is given by

$$T_{\boldsymbol{R}} = -\frac{\hbar^2}{2\mu}\Delta_{\boldsymbol{R}}, \tag{12}$$

with R being the relative coordinate between ^{11}Li and p and μ being the reduced mass. In the CDCC formalism, the total wave function in partial wave $J\pi$ is expanded as

$$\Psi^{JM\pi} = \frac{1}{R}\sum_{cLI} u^{J\pi}_{cLI}(R)\,\varphi^{JM\pi}_{cLI}(\Omega_R, \boldsymbol{x}, \boldsymbol{y}), \tag{13}$$

where the channel functions $\varphi^{JM\pi}_{cLI}$ are defined from

$$\varphi^{JM\pi}_{cLI}(\Omega_R, \boldsymbol{x}, \boldsymbol{y}) = \left[\left[\Psi^{j}_{3k}(\boldsymbol{x}, \boldsymbol{y}) \otimes \chi_p\right]^{I} \otimes Y_L(\Omega_R)\right]^{JM}. \tag{14}$$

In these definitions, k is the excitation level of ^{11}Li, χ_p is a spin-1/2 spinor, and index c stands for $c = (j, k)$. As I neglect the spin of the ^{9}Li core, $(j = 0^+, k = 1)$ represents the ground state. Other (j, k) values correspond to positive-energy states, and are therefore associated with pseudostates. In the CDCC theory, pseudostates are used to simulate breakup effects [16]. Individually, they depend on the choice of the basis, but the expansion (13) does not depend on the basis provided it is large enough.

The radial functions $u^{J\pi}_{cLI}(R)$ are obtained from a coupled-channel system which is solved by the R-matrix method [30,31]. This technique provides the scattering matrices for all J values, and therefore the elastic-scattering cross sections. Further details can be obtained in Ref. [30], for example.

The conditions of the calculation are similar to those of Ref. [14]. Typical values for the channel radius a and number of basis functions N are $a = 25$ fm and $N = 50$. Small variations around these values provide stable scattering matrices and cross sections. I include $j = 0^+, 1^-, 2^+, 3^-$ for ^{11}Li with pseudostates up to $E_{\text{max}} = 10$ MeV, which guarantees the convergence of the CDCC expansion. The $p + n$ and $p + {}^{9}$Li potentials are taken as the Minnesota interaction [32] and as the Koning-Delaroche parametrization [33], respectively. This model nicely reproduces the elastic cross section at $E_{\text{c.m.}} = 5.5$ MeV, where data are available [8]. It should be reliable at the present energy, $E_{\text{c.m.}} = 2.75$ MeV, which has been used in the $^{11}\text{Li}(p, t)\,^{9}\text{Li}$ experiment.

I present in Fig. 2 the elastic cross section in the single-channel approximation ("gs") and in the full CDCC model ("full"). As shown in Ref. [14], breakup channels have a significant effect, even if most of the corresponding channels are closed. A measurement of elastic cross sections, in parallel with other cross sections such as (p, t) would provide useful tests of the model.

At convergence, the number of channels [i.e., the number of (cLI) values in Eq. (13)] is very large (see Fig. 3 of Ref. [14]). In these conditions, the calculation of the $^{11}\text{Li}(p, t)\,^{9}\text{Li}$ cross section is extremely time-consuming.

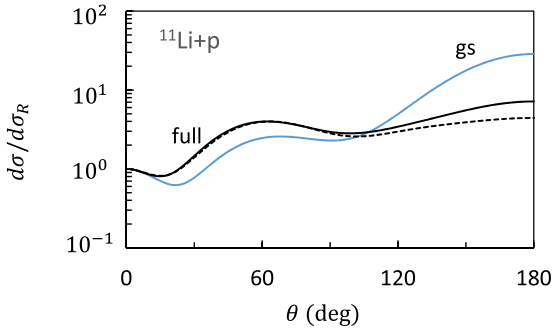

FIG. 2. ^{11}Li $+p$ elastic cross section (divided by the Rutherford cross section) at $E_{\rm c.m.} = 2.75$ MeV. The solid lines correspond to the full CDCC calculation (black) and to the single-channel approximation (blue). The dashed curve is obtained with the equivalent potential (see text).

To reduce the computer times, I have derived an equivalent potential from the CDCC results. This technique, proposed in Ref. [34], was adopted in several works, and in particular in the CDCC calculation of the ^{11}Li $+p$ cross section [14]. The idea is to replace the multichannel wave function (13) by a single-channel approximation

$$\Psi^{JM\pi} \approx \frac{1}{R} u_0^{J\pi}(R)\Psi_3^{0^+}(\boldsymbol{x},\boldsymbol{y})[\chi_p \otimes Y_L(\Omega_R)]^{JM}, \tag{15}$$

where the radial function $u_0^{J\pi}(R)$ is obtained from

$$\left[-\frac{\hbar^2}{2\mu}\left(\frac{d^2}{dR^2} - \frac{L(L+1)}{R^2}\right) + V_{\rm eq}(R) - E\right] u_0^{J\pi}(R) = 0. \tag{16}$$

In (16), $V_{\rm eq}(R)$ is a (complex) equivalent potential, derived from the multichannel problem (see details in Refs. [34,35]). This J-independent potential does not reproduce exactly the CDCC cross section. However, in most cases, it provides an excellent approximation. It is illustrated in Fig. 2 for the present system (dashed line). The main advantage of this technique is to provide a simpler single-channel approximation (15) which can be used in further applications. The equivalent potential at $E_{\rm c.m.} = 2.75$ MeV is similar to the one at $E_{\rm c.m.} = 5.5$ MeV, and I therefore refer to Ref. [14] [Fig. 6(a)] for further detail.

C. ^{9}Li $+t$ elastic scattering

There are no experimental data on ^{9}Li $+t$ elastic scattering. Consequently, and to be consistent with ^{11}Li $+p$, I determine the ^{9}Li $+t$ cross sections with the CDCC method. The technique is equivalent to the method presented in Sec. II B. The Hamiltonian involves the triton, described by a $p+n+n$ structure, and ^{9}Li $+p$ and ^{9}Li $+n$ optical potentials, taken from Ref. [33]. The CDCC elastic cross section is shown in Fig. 3(a) at a center-of-mass energy of $E_{\rm c.m.} =$ 10.8 MeV, which corresponds to the experimental conditions of Ref. [10]. As expected, breakup effects are small. I therefore neglect them in further calculations.

To test the sensitivity of the ^{9}Li $+t$ cross section in different conditions, I have also used the compilation of Pang *et al.*

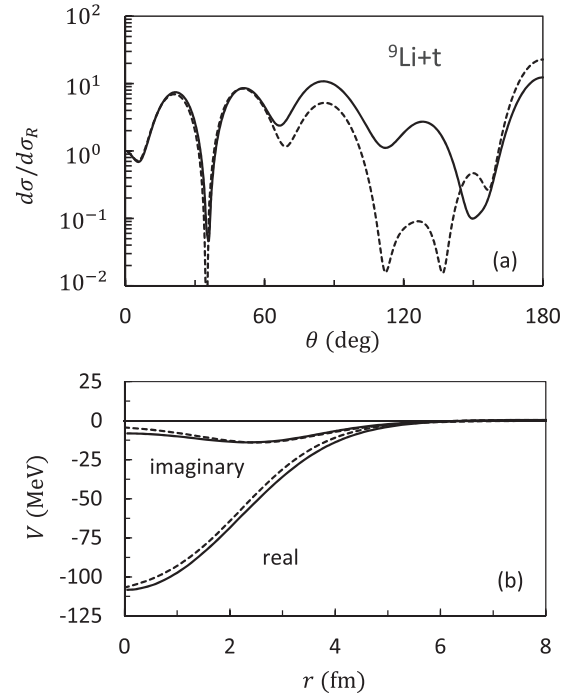

FIG. 3. (a) ^{9}Li $+t$ elastic cross section (divided by the Rutherford cross section) at $E_{\rm c.m.} = 10.8$ MeV. (b) Equivalent ^{9}Li $+t$ potentials. In both panels, the solid lines correspond to the CDCC calculation, and the dashed lines are obtained with the optical potential of Pang *et al.* [36].

[36]. The results are presented in Fig. 3(a) as a dashed line. Up to $\theta \approx 60^\circ$, both approaches provide quite similar cross sections, but they differ at larger angles. The corresponding scattering wave functions will be used in the study of the ^{11}Li$(p,t)^9$Li reaction.

As for ^{11}Li $+p$, I determine the ^{9}Li $+t$ equivalent potential, which is shown in Fig. 3(b). The potential deduced from the CDCC calculation is close to the global parametrization of Pang *et al.* [36].

III. DESCRIPTION OF THE ^{11}Li$(p,t)^9$Li TRANSFER

Here I use the ^{11}Li $+p$ and ^{9}Li $+t$ wave functions defined in Sec. II. At the DWBA, the transfer scattering matrix in partial wave $J\pi$ can be written as

$$U_{if}^{J\pi} = -\frac{i}{\hbar}\left\langle \Psi_f^{JM\pi(-)} \middle| \Delta V + V_{\rm rem} \middle| \Psi_i^{JM\pi(+)} \right\rangle, \tag{17}$$

where $\Psi_i^{JM\pi(+)}$ and $\Psi_f^{JM\pi(-)}$ are the ^{11}Li $+p$ and ^{9}Li $+t$ scattering wave functions [19]. The residual interaction ΔV and the remnant term are defined as

$$\begin{aligned} \Delta V &= V_{p+n_1} + V_{p+n_2}, \\ V_{\rm rem} &= V_{^9{\rm Li}+p} - V_{^{11}{\rm Li}+p} \end{aligned} \tag{18}$$

for the prior form, and by

$$\begin{aligned} \Delta V &= V_{^9{\rm Li}+n_1} + V_{^9{\rm Li}+n_2}, \\ V_{\rm rem} &= V_{^9{\rm Li}+p} - V_{^9{\rm Li}+t} \end{aligned} \tag{19}$$

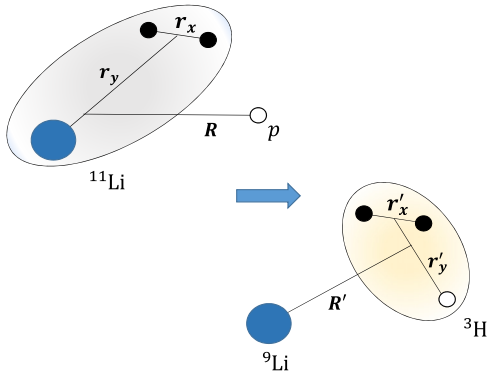

FIG. 4. Coordinates used in the present model. Two neutrons from ^{11}Li are transferred to the proton.

for the post form. All potentials depend on the various coordinates $(\boldsymbol{R}, \boldsymbol{r}_x, \boldsymbol{r}_y, \boldsymbol{R}', \boldsymbol{r}'_x, \boldsymbol{r}'_y)$, as shown in Fig. 4. The integrals involved in definition (17) are performed, either over $(R, \boldsymbol{r}_x, \boldsymbol{r}_y)$ or over (R', r'_x, r'_y). In practice, however, they are replaced by integrals over $(\boldsymbol{r}_x, R, R')$ with

$$\begin{aligned} \boldsymbol{r}'_x &= \boldsymbol{r}_x, \\ \boldsymbol{r}_y &= \frac{A_1+2}{3A_1+4}(3\boldsymbol{R}' - \boldsymbol{R}), \\ \boldsymbol{r}'_y &= \frac{3}{3A_1+4}(2\boldsymbol{R}' - (A_1+2)\boldsymbol{R}). \end{aligned} \tag{20}$$

As long as the scattering wave functions $\Psi_i^{JM\pi(+)}$ and $\Psi_f^{JM\pi(-)}$ are exact, the post and prior forms are equivalent. The comparison of the cross sections obtained with both forms provides an excellent test of the calculation. Depending on the reaction, the remnant term may be negligible in one of the forms. For example, in the $A(d,p)A'$ transfer reaction (with $A' = A+1$), the remnant term in the prior form is $V_{\rm rem} = V_{p+A} - V_{d+A}$ whereas it is $V_{\rm rem} = V_{p+A} - V_{p+A'}$ in the post form. It is clear that, for large A, $V_{p+A} \approx V_{p+A'}$ and the remnant term can be neglected in the post form. In the present (p,t) reaction, I expect a smaller remnant term in the prior form.

The scattering matrix (17) can be reformulated as

$$U_{if}^{J\pi} = -\frac{i}{\hbar}\int u_{L_i}^{J\pi}(R)\,\mathcal{K}_{L_iL_f}^{J\pi}(R,R')\,u_{L_f}^{J\pi}(R')dRdR', \tag{21}$$

where $u_{L_i}^{J\pi}(R)$ and $u_{L_f}^{J\pi}(R')$ are the relative wave functions of the ^{11}Li $+\,p$ and ^{9}Li $+\,t$ systems. As I use the CDCC equivalent potentials, the scattering wave functions only contain one channel with $I = 1/2$, $L = J \pm 1/2$. The transfer kernel $\mathcal{K}_{L_iL_f}^{J\pi}(R,R')$ is defined by

$$\begin{aligned} \mathcal{K}_{L_iL_f}^{J\pi}(R,R') = \mathcal{J}\big\langle \big[\Psi_{3(t)}^{1/2+}(\boldsymbol{r}'_x,\boldsymbol{r}'_y)\otimes Y_{L_f}(\Omega_{R'})\big]^J \\ |\Delta V + V_{\rm rem}|\Psi_{3({\rm Li})}^{0+}(\boldsymbol{r}_x,\boldsymbol{r}_y)\big[Y_{L_i}(\Omega_R)\otimes\chi_p\big]^J\big\rangle, \end{aligned} \tag{22}$$

where $\mathcal{J}$ is the Jacobian, and $\Psi_{3({\rm Li})}^{0+}$ and $\Psi_{3(t)}^{1/2+}$ are the ^{11}Li and ^{3}H three-body wave functions, defined in Sec. II A. The calculation is presented in the Appendix. Although the general formulation (21) is common, the calculation of the kernels is more complicated than in standard DWBA calculations, where a single particle is transferred (see, for example, Ref. [37]). The use of three-body wave functions for ^{11}Li and ^{3}H makes the calculations more difficult since more variables are involved. A similar, though simplified, calculation has been performed in Ref. [38] for the ^{6}He$(p,t)\alpha$ reaction.

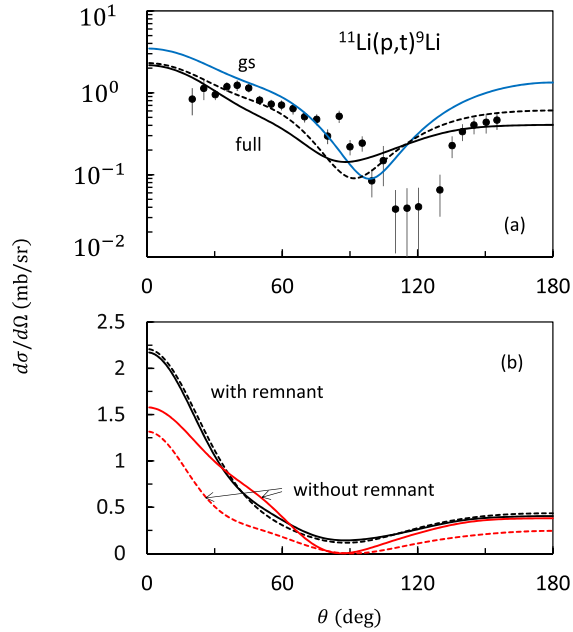

FIG. 5. (a) ^{11}Li$(p,t)\,^{9}$Li cross section with the full CDCC model (solid black) and with the single-channel approximation (solid blue). The dashed line is obtained with the ^{9}Li $+\,t$ optical potential of Ref. [36]. The data are taken from Ref. [10]. (b) CDCC calculations with and without the remnant term. The solid lines correspond to the prior form and the dashed lines to the post form.

IV. THE ^{11}Li$(p,t)\,^{9}$Li REACTION

A. Cross sections

The transfer cross section is computed from the scattering matrices (17) up to $J_{\rm max} = 15/2$ and is presented in Fig. 5. Let me stress that there is no adjustable parameter in the model. A first calculation is performed with the ^{11}Li ground state only [blue line in Fig. 5(a)]. At small angles, it overestimates the experimental data of Ref. [10]. Although the theoretical description is not perfect, the presence of breakup channels in the full CDCC calculation reduces the cross section, except near the minimum around $\theta \approx 90^\circ$.

As the ^{9}Li $+\,t$ scattering wave functions cannot be tested through experimental cross sections, I have also used the potential of Pang *et al.* [36] instead of the ^{9}Li $+\,t$ four-body CDCC model. The results [dashed line in Fig. 5(a)] show that the difference is small.

In Fig. 5(b), I display the ^{11}Li$(p,t)\,^{9}$Li cross section with and without the remnant term. When the remnant term is included, the cross sections in both forms are almost indistinguishable. As expected, the prior form gives a better approximation than the post form when the remnant term

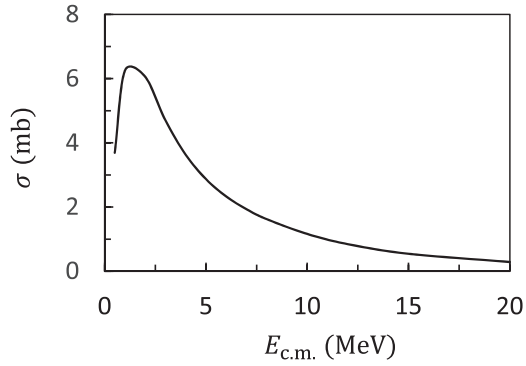

FIG. 6. Integrated cross section (23) for the ^{11}Li$(p,t)^{9}$Li reaction.

is neglected. However, an accurate calculation requires the introduction of the remnant term in any form. This term is included in all transfer calculations.

The integrated cross section is presented Fig. 6 for c.m. energies up to 20 MeV. The integrated cross section is defined as

$$\sigma(E) = \frac{\pi}{2k^2}\sum_{J\pi}(2J+1)\left|U_L^{J\pi}\right|^2, \tag{23}$$

where the scattering matrices (17) are used. Figure 6 suggests that a maximum is obtained near $E_{\rm c.m.} = 2.5$ MeV, which nearly corresponds to the energy considered in the experiment of Ref. [10].

In order to have a better insight on the J dependence of the cross section, I plot in Fig. 7 the quantity $(2J+1)|U_L^{J\pi}|^2$, which is involved in the integrated cross section, as a function of L. At $E_{\rm c.m.} = 2.75$ MeV, the maximum is obtained for $L = 1$. Owing to the low incident energy, only low L values are involved. Partial waves beyond $L = 4$ are negligible.

B. Halo effects

The ^{11}Li nucleus is well known to present a marked halo structure, with two neutrons located far from the ^{9}Li core. In order to highlight this halo effect in the ^{11}Li$(p,t)^{9}$Li reaction, I have set an upper value, denoted as $\rho_{\rm max}$ on the hyper-radius. This means that, in the calculation of the $N^{\lambda}_{cc'}(R,R')$ functions [see Eq. (A12)] the hyper-radial functions $\chi^{J\pi}_{\gamma K}(\rho)$ have been set to zero for $\rho \geqslant \rho_{\rm max}$. This method, although indirect, provides information on the role of large distances in ^{11}Li, and therefore on its halo structure.

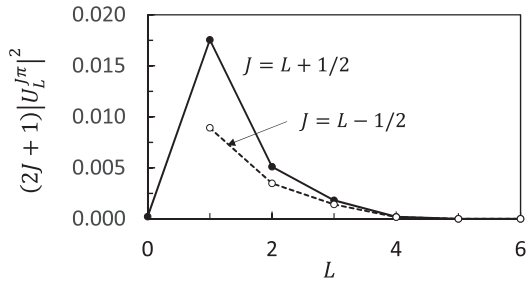

FIG. 7. Square modulus of the transfer scattering matrix [times $(2J+1)$] as a function of the initial angular momentum L.

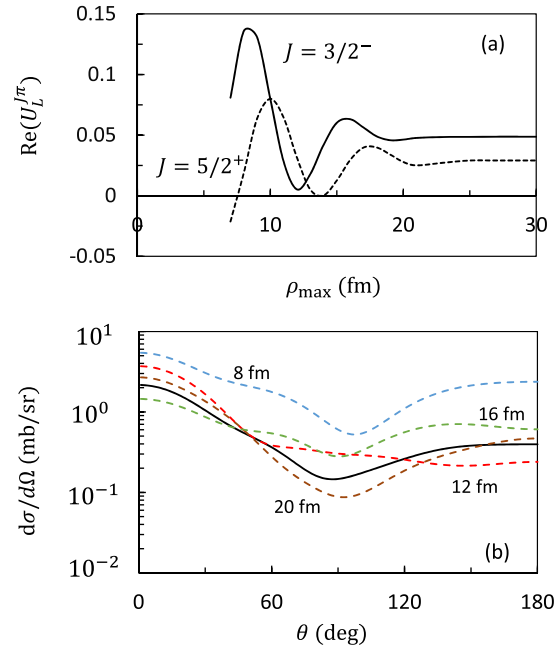

FIG. 8. Influence of $\rho_{\rm max}$ on the ^{11}Li$(p,t)^{9}$Li transfer (see text). (a) Real part of the $3/2^-$ and $5/2^+$ scattering matrices as a function of $\rho_{\rm max}$. (b) Differential cross section for various $\rho_{\rm max}$ values (labels).

The influence of $\rho_{\rm max}$ is shown in Fig. 8, where I plot the real part of the scattering matrix for two typical partial waves, $J = 3/2^-$ and $J = 5/2^+$. Clearly, large ρ values are necessary to reach convergence. This could be expected from the ^{11}Li wave function [Fig. 1(a)], which decreases slowly at large distances. The same conclusion can be drawn from Fig. 8(b), where the cross section is plotted for various $\rho_{\rm max}$ values. This figure confirms the strong sensitivity to the long-range part of the ^{11}Li wave function.

In Fig. 9, I plot the integrand of the transfer scattering matrix (17) (real part) for $J = 3/2^-$, which is the dominant partial wave. As expected, this integrand is dominant for $R \approx R'$. Of course, the transfer kernel $\mathcal{K}^{J\pi}(R,R')$ is significant at short distances only, but the initial and final scattering wave functions make this integrand quite complicated, with positive and negative values. The double integral in Eq. (17) must

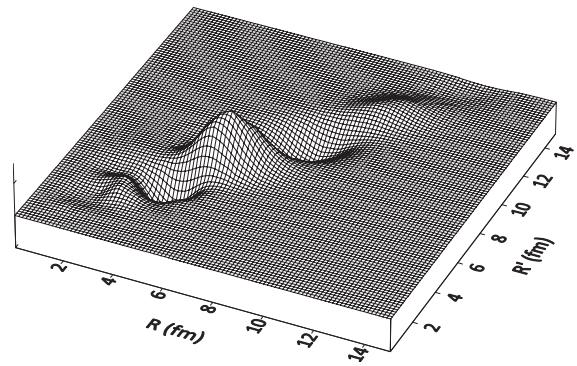

FIG. 9. Integrand of the scattering matrix (17) (real part) for $J = 3/2^-$. The units are arbitrary.

be performed up to $R, R' \approx 15$ fm to get accurate scattering matrices.

V. CONCLUSION

I have presented a CDCC calculation of the ^{11}Li$(p,t)^{9}$Li transfer cross section, which has been measured at $E_{\rm lab} = 33$ MeV [10]. The three-body structure of ^{11}Li is taken into account through a ^{9}Li $+n+n$ model which reproduces fairly well the experimental rms radius (the two-neutron separation energy is adjusted by a scaling factor applied to the ^{9}Li $+n$ potential, but this factor is very close to 1). The breakup of ^{11}Li is simulated by including pseudostates. In Ref. [14], this approach provided an excellent description of ^{11}Li $+p$ elastic scattering at $E_{\rm lab} = 66$ MeV.

Since two neutrons are transferred from ^{11}Li, a consistent description of ^{3}H requires a $p+n+n$ three-nucleon model. In the ^{9}Li $+t$ elastic scattering, however, breakup effects play a minor role. I have developed the formalism of two-neutron transfer at the DWBA. It represents an extension of the more frequent one-neutron transfer, but the calculations are much more involved. To decrease the computer times, I have determined ^{11}Li $+p$ and ^{9}Li $+t$ equivalent potentials, which reduces the DWBA calculation to a single-channel problem.

The ^{11}Li$(p,t)^{9}$Li cross section is in reasonable agreement with experiment, considering that there is no adjustable parameter. At small angles, the angular distribution is reduced by ^{11}Li breakup effects, which is supported by the experimental data. A possible improvement would be to introduce the core excitation in the ^{11}Li description, but this would make the calculation even more difficult. In addition, this extension would involve various potentials (^{9}Li$^{\star} + n$, ^{9}Li$^{\star} + p$), which are poorly known or even unknown.

I have shown that the transfer process is sensitive to the halo structure of ^{11}Li since the cross section sensitively depends on the large distance contribution. This approach seems therefore promising to test the long-range structure of halo nuclei. Experimental data at higher energies would be welcome to further test the models, for scattering as well as for spectroscopy. In addition, a measurement of ^{11}Li $+p$ elastic scattering is also an important constraint for the theory and, if possible, should be studied in parallel with the transfer reaction.

ACKNOWLEDGMENTS

This work was supported by the Fonds de la Recherche Scientifique (FNRS) under Grants No. 4.45.10.08 and No. J.0049.19. It benefited from computational resources made available on the Tier-1 supercomputer of the Fédération Wallonie-Bruxelles, infrastructure funded by the Walloon Region under Grant Agreement No. 1117545.

APPENDIX: CALCULATION OF THE TWO-NEUTRON TRANSFER KERNEL

In this Appendix, I give technical information on the transfer kernel (22). The various potentials in (18) depend on coordinates $(\boldsymbol{R}, \boldsymbol{r}_x, \boldsymbol{r}_y, \boldsymbol{R}', \boldsymbol{r}'_x, \boldsymbol{r}'_y)$, and the integrals in (22) are performed over $\boldsymbol{r}_x$ (or $\boldsymbol{r}'_x$), Ω_R, and $\Omega_{R'}$. Let me discuss the prior form (18). The potential $V_{^{9}\mathrm{Li}+p}$ only depends on $\boldsymbol{R}'$ and $\boldsymbol{r}'_y$, whereas $V_{^{11}\mathrm{Li}+p}$ depends on $\boldsymbol{R}'$. The V_{p+n_1} and V_{p+n_2} potentials are more complicated since they depend on $\boldsymbol{r}'_x$ and $\boldsymbol{r}'_y$. It is, however, possible to replace these terms by using the three-body Eq. (1) for ^{3}H. In the hyperspherical expansion, I have

$$\big(V_{p+n_1} + V_{p+n_2}\big)\chi^{j\pi}_{\gamma K} = \big(E_3 - T - V_{n_1+n_2}\big)\chi^{j\pi}_{\gamma K}, \tag{A1}$$

where E_3 is the ^{3}H binding energy, and T is the kinetic-energy operator defined by

$$T\,\chi^{j\pi}_{\gamma K} = -\frac{\hbar^2}{2m_N}\left(\frac{d^2}{d\rho^2} - \frac{(K+3/2)(K+5/2)}{\rho^2}\right)\chi^{j\pi}_{\gamma K}, \tag{A2}$$

where m_N is the nucleon mass. The advantage of Eq. (A1) is that the $V_{n_1+n_2}$ potential depends on $\boldsymbol{r}_x$ only. This permits a significant simplification of the calculations.

The next step is to write the ^{11}Li wave functions as

$$\Psi^{jm}_{3(\mathrm{Li})}(\boldsymbol{r}_x, \boldsymbol{r}_y) = \sum_c \Phi^{j}_{11,c}(r_x, r_y)\varphi^{jm}_{11,c}(\Omega_x, \Omega_y), \tag{A3}$$

where index c stands for $c = (\ell_x, S_{12}, j_x, \ell_y)$ and where the angular part reads

$$\varphi^{jm}_{11,c}(\Omega_x, \Omega_y) = \big[\big[Y_{\ell_x}(\Omega_x) \otimes S_{12}\big]^{j_x} \otimes Y_{\ell_y}(\Omega_y)\big]^{jm}. \tag{A4}$$

The radial components are given by

$$\Phi^{j}_{11,c}(r_x, r_y) = \sum_K \chi^{j\pi}_{cK}(\rho)\Phi^{\ell_x\ell_y}_K(\alpha), \tag{A5}$$

where ρ and α are related to $(\boldsymbol{r}_x, \boldsymbol{r}_y)$ with Eqs. (2) and (4). The ^{11}Li $+p$ scattering wave function (13) is then rewritten as

$$\Psi^{JM\pi}_i = \sum_{cL_iI_i} \Phi^{j}_{11,c}(r_x, r_y)\big[\big[\varphi^{j}_{11,c}(\Omega_x, \Omega_y) \otimes S_3\big]^{I_i} \otimes Y_{L_i}(\Omega_R)\big]^{JM}. \tag{A6}$$

Similarly, the ^{3}H wave function is written as

$$\Psi^{j'm'}_{3(t)}(\boldsymbol{r}'_x, \boldsymbol{r}'_y) = \sum_{c'} \Phi^{j'}_{3,c}(r'_x, r'_y)\varphi^{j'm'}_{3,c'}(\Omega'_x, \Omega'_y), \tag{A7}$$

with

$$\varphi^{j'm'}_{3,c'}(\Omega'_x, \Omega'_y) = \big[\big[Y_{\ell'_x}(\Omega'_x) \otimes S_{12}\big]^{j'_x} \otimes \big[Y_{\ell'_y}(\Omega'_y) \otimes S_3\big]^{j'_y}\big]^{j'm'}. \tag{A8}$$

The ^{9}Li $+t$ scattering wave function in the final state is therefore given by

$$\Psi^{JM\pi}_f = \sum_{c'L_f} \Phi^{j'}_{3,c}(r'_x, r'_y)\big[\varphi^{j'}_{3,c'}(\Omega'_x, \Omega'_y) \otimes Y_{L_f}(\Omega'_R)\big]^{JM}, \tag{A9}$$

since the ^{9}Li spin is neglected.

The calculation of the transfer kernel (21) is done by factorizing the radial and angular parts. The main issue is that $\boldsymbol{r}_y$ and r'_y must be expressed as functions of R and of R'. This is done with Eqs. (20) and with the expansion

$$S^L Y^M_L(\Omega_S) = \sum_k C^L_k(\alpha\boldsymbol{r}_1)^k(\beta\boldsymbol{r}_2)^{L-k}[Y_k(\Omega_1) \otimes Y_{L-k}(\Omega_2)]^{LM}, \tag{A10}$$

where

$$\boldsymbol{S} = \alpha \boldsymbol{r}_1 + \beta \boldsymbol{r}_2,$$
$$C_k^L = \left(\frac{4\pi (2L+1)!}{(2k+1)!(2L-2k+1)!} \right)^{1/2}. \quad \text{(A11)}$$

For the radial part of the transfer kernel, I expand

$$\int \frac{\Phi^j_{11,c}(\boldsymbol{r}_x, \boldsymbol{r}_y)}{\boldsymbol{r}_y^{\ell_y+1}} (\Delta V + V_{\rm rem}) \frac{\Phi^{j'}_{3,c'}(r'_x, r'_y)}{\boldsymbol{r}_{y'}^{\ell'_y+1}} \boldsymbol{r}_x^2 d\boldsymbol{r}_x$$
$$= \sum_\lambda N^\lambda_{cc'}(R, R') P_\lambda(\cos\theta), \quad \text{(A12)}$$

where Eqs. (A1) and (A2) are used, and where θ is the angle between $\boldsymbol{R}$ and $\boldsymbol{R}'$. As $V_{n_1+n_2}$ does not depend on $\Omega_{x'}$, the integration over $\boldsymbol{r}_x = r'_x$ can easily be done numerically (through a Gauss-Laguerre quadrature).

The kernel for a two-neutron transfer can be generalized from the one-neutron transfer kernel (see, for example, Eq. (8) of Ref. [37]) as

$$\mathcal{K}^{J\pi}_{L_i L_f} = \sum_{k_1 k_2 \lambda c c'} F^{J\pi}_{L_i L_f, k_1 k_2 \lambda c c'} I_{k_1 k_2 \lambda c c'}(R, R'), \quad \text{(A13)}$$

where functions $I_{k_1 k_2 \lambda c c'}(R, R')$ are given by

$$I_{k_1 k_2 \lambda c c'}(R, R') = C_{k_1}^{\ell_y} C_{k_2}^{\ell'_y} (\alpha R)^{k_1} (\beta R')^{\ell_y - k_1} (\gamma R)^{k_2}$$
$$\times (\delta R')^{\ell'_y - k_2} N^\lambda_{cc'}(R, R'). \quad \text{(A14)}$$

They only depend on the internal wave functions of ^{11}Li and of ^{3}H, but not on the total spin J and on the relative angular momenta L_i and L_f. The coefficients $F^{J\pi}_{L_i L_f, k_1 k_2 \lambda c c'}$ can be calculated analytically from the matrix elements between the angular components of (A6) and (A9) as

$$F^{J\pi}_{L_i L_f, k_1 k_2 \lambda c c'} = \langle \psi_f | P_\lambda | \psi_i \rangle, \quad \text{(A15)}$$

where ψ_i and ψ_f are shorthand notations for

$$\psi_i = \Big[\Big[\Big[Y^{j_x}_{\ell_x S_{12}}(\Omega_x) \otimes Y^{\ell_y}_{k_1 \ell_y - k_1}(\Omega_R, \Omega'_R) \Big]^j \otimes S_3 \Big]^{I_i}$$
$$\otimes Y_{L_i}(\Omega_R) \Big]^{JM},$$
$$\psi_f = \Big[\Big[Y^{j'_x}_{\ell'_x S_{12}}(\Omega'_x) \otimes \Big[Y^{\ell'_y}_{k_2 \ell'_y - k_2}(\Omega_R, \Omega'_R) \otimes S_3 \Big]^{j'_y} \Big]^{j'}$$
$$\otimes Y_{L_f}(\Omega'_R) \Big]^{JM}. \quad \text{(A16)}$$

In these equations, I define

$$Y^{jm}_{\ell S_{12}}(\Omega_x) = [Y_\ell(\Omega_x) \otimes S_{12}]^{jm},$$
$$Y^{\ell m}_{\ell_a \ell_b}(\Omega_R, \Omega'_R) = \big[Y_{\ell_a}(\Omega_R) \otimes Y_{\ell_b}(\Omega'_R) \big]^{\ell m}. \quad \text{(A17)}$$

The calculation of the angular matrix elements (A15) involves many coupling coefficients, but can be performed analytically. Again, this definition represents a generalization of a one-nucleon transfer (see Eq. (A10) of Ref. [37]).

[1] I. Tanihata, H. Savajols, and R. Kanungo, Prog. Part. Nucl. Phys. **68**, 215 (2013).
[2] I. Tanihata, H. Hamagaki, O. Hashimoto, Y. Shida, N. Yoshikawa, K. Sugimoto, O. Yamakawa, T. Kobayashi, and N. Takahashi, Phys. Rev. Lett. **55**, 2676 (1985).
[3] C. Bachelet, G. Audi, C. Gaulard, C. Guénaut, F. Herfurth, D. Lunney, M. de Saint Simon, and C. Thibault, Phys. Rev. Lett. **100**, 182501 (2008).
[4] I. Tanihata, T. Kobayashi, O. Yamakawa, S. Shimoura, K. Ekuni, K. Sugimoto, N. Takahashi, T. Shimoda, and H. Sato, Phys. Lett. B **206**, 592 (1988).
[5] P. Egelhof, G. Alkhazov, M. Andronenko, A. Bauchet, A. Dobrovolsky, S. Fritz, G. Gavrilov, H. Geissel, C. Gross, A. Khanzadeev, G. Korolev, G. Kraus, A. Lobodenko, G. Münzenberg, M. Mutterer, S. Neumaier, T. Schäfer, C. Scheidenberger, D. Seliverstov, N. Timofeev *et al.*, Eur. Phys. J. A **15**, 27 (2002).
[6] N. Alamanos, C. Bertulani, A. Bonaccorso, A. Bracco, D. M. Brink, and G. Casini, Eur. Phys. J. Plus **132**, 37 (2017).
[7] J. P. Fernández-García, M. Cubero, L. Acosta, M. Alcorta, M. A. G. Alvarez, M. J. G. Borge, L. Buchmann, C. A. Diget, H. A. Falou, B. Fulton, H. O. U. Fynbo, D. Galaviz, J. Gómez-Camacho, R. Kanungo, J. A. Lay, M. Madurga, I. Martel, A. M. Moro, I. Mukha, T. Nilsson *et al.*, Phys. Rev. C **92**, 044608 (2015).
[8] J. Tanaka, R. Kanungo, M. Alcorta, N. Aoi, H. Bidaman, C. Burbadge, G. Christian, S. Cruz, B. Davids, A. D. Varela, J. Even, G. Hackman, M. Harakeh, J. Henderson, S. Ishimoto, S. Kaur, M. Keefe, R. Krücken, K. Leach, J. Lighthall *et al.*, Phys. Lett. B **774**, 268 (2017).
[9] T. Nakamura, A. M. Vinodkumar, T. Sugimoto, N. Aoi, H. Baba, D. Bazin, N. Fukuda, T. Gomi, H. Hasegawa, N. Imai, M. Ishihara, T. Kobayashi, Y. Kondo, T. Kubo, M. Miura, T. Motobayashi, H. Otsu, A. Saito, H. Sakurai, S. Shimoura *et al.*, Phys. Rev. Lett. **96**, 252502 (2006).
[10] I. Tanihata, M. Alcorta, D. Bandyopadhyay, R. Bieri, L. Buchmann, B. Davids, N. Galinski, D. Howell, W. Mills, S. Mythili, R. Openshaw, E. Padilla-Rodal, G. Ruprecht, G. Shiffer, A. C. Shotter, M. Trinczek, P. Walden, H. Savajols, T. Roger, M. Caamano *et al.*, Phys. Rev. Lett. **100**, 192502 (2008).
[11] R. Ascuitto, N. K. Glendenning, and B. Sørensen, Nucl. Phys. A **183**, 60 (1972).
[12] N. K. Glendenning and G. Wolschin, Nucl. Phys. A **269**, 223 (1976).
[13] T. Takemasa, Phys. Rev. C **18**, 1677 (1978).
[14] P. Descouvemont, Phys. Rev. C **101**, 064611 (2020).
[15] G. H. Rawitscher, Phys. Rev. C **9**, 2210 (1974).
[16] N. Austern, Y. Iseri, M. Kamimura, M. Kawai, G. Rawitscher, and M. Yahiro, Phys. Rep. **154**, 125 (1987).
[17] T. Matsumoto, E. Hiyama, K. Ogata, Y. Iseri, M. Kamimura, S. Chiba, and M. Yahiro, Phys. Rev. C **70**, 061601(R) (2004).
[18] M. Rodríguez-Gallardo, J. M. Arias, J. Gómez-Camacho, R. C. Johnson, A. M. Moro, I. J. Thompson, and J. A. Tostevin, Phys. Rev. C **77**, 064609 (2008).
[19] G. R. Satchler, *Direct Nuclear Reactions* (Oxford University Press, Oxford, UK, 1983).

[20] A. M. Moro, F. M. Nunes, and R. C. Johnson, Phys. Rev. C **80**, 064606 (2009).
[21] N. Timofeyuk and R. Johnson, Prog. Part. Nucl. Phys. **111**, 103738 (2020).
[22] M. V. Zhukov, B. V. Danilin, D. V. Fedorov, J. M. Bang, I. J. Thompson, and J. S. Vaagen, Phys. Rep. **231**, 151 (1993).
[23] C. D. Lin, Phys. Rep. **257**, 1 (1995).
[24] P. Descouvemont, C. Daniel, and D. Baye, Phys. Rev. C **67**, 044309 (2003).
[25] D. Baye, Phys. Rep. **565**, 1 (2015).
[26] E. C. Pinilla, P. Descouvemont, and D. Baye, Phys. Rev. C **85**, 054610 (2012).
[27] H. Esbensen, G. F. Bertsch, and K. Hencken, Phys. Rev. C **56**, 3054 (1997).
[28] Y. Suzuki, W. Horiuchi, M. Orabi, and K. Arai, Few-Body Syst. **42**, 33 (2008).
[29] P. Descouvemont, E. M. Tursunov, and D. Baye, Nucl. Phys. A **765**, 370 (2006).
[30] P. Descouvemont and D. Baye, Rep. Prog. Phys. **73**, 036301 (2010).
[31] P. Descouvemont, Comput. Phys. Commun. **200**, 199 (2016).
[32] D. R. Thompson, M. LeMere, and Y. C. Tang, Nucl. Phys. A **286**, 53 (1977).
[33] A. J. Koning and J. P. Delaroche, Nucl. Phys. A **713**, 231 (2003).
[34] I. Thompson, M. Nagarajan, J. Lilley, and M. Smithson, Nucl. Phys. A **505**, 84 (1989).
[35] P. Descouvemont, Phys. Rev. C **97**, 064607 (2018).
[36] D. Y. Pang, P. Roussel-Chomaz, H. Savajols, R. L. Varner, and R. Wolski, Phys. Rev. C **79**, 024615 (2009).
[37] Shubhchintak and P. Descouvemont, Phys. Rev. C **100**, 034611 (2019).
[38] Y. T. Oganessian, V. I. Zagrebaev, and J. S. Vaagen, Phys. Rev. C **60**, 044605 (1999).